Supplementary Information

Mechanism of misfolding of the human prion protein revealed by a pathological mutation

Máximo Sanz-Hernández[1], Joseph D. Barritt[1], Jens Sobek[2], Simone Hornemann[3], Adriano Aguzzi[3], Alfonso De Simone*[1,4]

[1]Department of Life Sciences, Imperial College London, South Kensington, SW7 2AZ UK; [2]Functional Genomics Center Zurich, Eidgenössische Technische Hochschule (ETH) Zurich and University of Zurich, Zurich, Switzerland; [3]Institute of Neuropathology, University of Zurich, Zurich, Switzerland; [4]Department of Pharmacy, University of Naples "Federico II", Naples, Italy

* Alfonso De Simone
Email: a.de-simon@imperial.ac.uk

This PDF file includes:

SI Methods

huPrP$^{C}_{125\text{-}230}$ expression and purification. The sequences of wild-type (WT) and T183A huPrP$^{C}_{125\text{-}230}$ were cloned into pET-15b protein expression vectors (Novagen, Merck Millipore, UK) with an N-terminal 6xHis tag and modified to contain a Tobacco Etch Virus (TEV) protease cleavage site. The plasmids were transformed into BL21 (DE3) pLysS competent cells (Invitrogen, Thermo Fisher Scientific, UK), which were grown at 37°C in 2xTY growth medium and induced with 1 mM isopropyl β-D-1-thiogalactopyranoside (IPTG) when an OD_{600} value of 1.5 was reached. For isotopically labeled proteins in NMR experiments, cells were transferred at this stage to M9 growth medium supplemented with 0.7 grams/litre $^{15}NH_4Cl$ (Cambridge Isotope Laboratories, UK) and 2.0 grams/litre ^{13}C D-glucose (Cambridge Isotope Laboratories, UK). The transfer was performed by gentle centrifugation in a Beckman Coulter Avanti J-E high speed centrifuge (F10-6x500y rotor) at 1500 RCF for 10 minutes at 4°C, and subsequent resuspension. Protein expression was carried out over 4 hours, at 37°C. Cells were then harvested by centrifugation in the same equipment (4000 RCF, 10 minutes, 4°C).

huPrP$^{C}_{125\text{-}230}$ was expressed insolubly and purified from inclusion bodies. Cell pellets were solubilized in lysis buffer (100 mM Na_2HPO_4, 250 mM NaCl, 2 mM DTT, pH 8.0) and sonicated by applying 3 rounds of 30 seconds (0.5 seconds on, 0.5 seconds off) while kept on ice. The lysate was centrifuged at 20000 RCF (F21-8x50y rotor), 4°C for 30 minutes, and the pellet containing the inclusion bodies solubilized in Lysis buffer + 1% Triton X-100 (Sigma-Aldrich, UK), followed by repeated centrifugation, resuspension in Lysis buffer and centrifugation using the same setup. The washed inclusion bodies were then solubilized using 6M Guanidine Hydrochloride, 100 mM Na_2HPO_4, 10 mM reduced L-glutathione, pH 8.0.

Solubilized huPrP$^{C}_{125\text{-}230}$ was bound to Ni-NTA agarose affinity resin (Sigma-Aldrich, UK), incubated with 20 mM imidazole to remove unspecific binding and eluted with 150 mM imidazole. The eluted fractions were dialyzed into a buffer containing 4 M Guanidine Hydrochloride, 100 mM Na_2HPO_4, pH 7.0. Refolding was carried out at 4°C by drop-wise dilution into a buffer composed of 100 mM Na_2HPO_4, pH 7.0, at a 1:20 dilution factor. The 6xHis tag was cleaved by overnight incubation at 4°C with TEV protease (recombinantly produced in-house) at a 1:20 protein:protease molar ratio, and the cleaved protein was further purified by collecting the flow-through after 1 hour incubation with Ni-NTA Agarose resin. The final product was further purified by size exclusion using a Superdex 75 100/300

GL column (GE Healthcare, UK), in order to ensure their correct and monomeric refolding. The final huPrP$^{C}_{125\text{-}230}$ samples were concentrated up to 100 μM using an Amicon 200 ml stirred ultrafiltration cell equipped with 3 kDa NMW ultrafiltration discs (Merck Millipore, UK).

After each step, the purity of samples was evaluated by SDS-PAGE and the protein concentration determined from absorbance at 280 nm measured on a NanoDrop 1000 instrument (Thermo Fisher Scientific, UK) using an extinction coefficient of 16,500 M^{-1} cm^{-1}.

Nuclear magnetic resonance. The assignment of WT and T183A backbone resonances was performed using a combination of three-dimensional spectra to evaluate sequential residue connectivities (1), resulting in the assignment of 92% and 86% of non-proline residues in WT of T183A constructs, respectively. Assignment for both proteins was performed using an 800 MHz Avance III HD Bruker spectrometer with cryoprobe TCI. Measurements were made at 16°C, pH 7.0 in 100 mM Na_2HPO_4 (10% D_2O) buffer at protein concentration of 130 μM. CPMG experiments were run at two spectrometer frequencies (800MHz and 950 MHz) using Avance III HD Bruker spectrometers with cryoprobe TCI. Experiments were set with a constant-time relaxation interval (2) T_{relax} of 40 ms. 16 different ν_{CPMG} values were sampled ranging from 50 to 1200 Hz, and measurements were run in triplicates.

NMR data were processed using the NMRpipe software (3), and relaxation dispersion profiles were fitted to a two-state chemical exchange model (4) using the Relax software package (5). Analyses of secondary structure populations based on chemical shifts were performed using the δ2D method (6). Chemical shift perturbations ($\Delta\delta$) were computed on the ^{1}H-^{15}N HSQC spectra by calculating the Pythagorean distance between shifts, by scaling the ^{15}N changes using a factor of 0.14 (7).

Metadynamics simulations. The intermediate, sub-millisecond conformational exchange identified by NMR can be classified as a highly rare event in the timescales that are generally accessible by full-atomic molecular dynamics sampling. A very well established technique that can enhance the sampling of such rare events is metadynamics (8). Metadynamics relies on the definition of so-called collective variables (CVs), which are functions of the atomic coordinates that describe the conformational properties of the system. CVs are biased over time in order to achieve an extensive sampling of their configurational space. We specifically employed a bias-exchange metadynamics

approach (9), whereby different replicas are run in parallel, individually biased on different CVs, and random exchanges occur periodically.

In our sampling of wild-type and T183A huPrP$^{C}_{125\text{-}230}$, five different replicas were run. The five collective variables employed were:

CV1. Cα-Root Mean Square Deviation (RMSD) from the native structure. This was computed on the Cα atoms of the S1-H1-H2 subdomain (residues 125-169) by aligning the protein structure using the Cα atoms of the H2-H3 subdomain (residues 170-230).

CV2. Radius of gyration.

CV3. Total α-helical content (determined as a summation of the normalized RMSD to an ideal helix of every six-residue segment in the protein (10)).

CV4. Distance from the center of mass of helix-1 (residues 148-152) to the center of mass of the disulphide bridge at the core of H2-H3 (residues 178-180 and 213-215).

CV5. Number of Cα contacts between subdomains S1-H1-S2 (residues 125-169) and H2-H3 (170-230). Residues 167-174 were excluded from this variable to avoid artifactual contacts due to close sequence proximity.

These CVs have been carefully chosen to distinguish between the native conformation of huPrP$^{C}_{125\text{-}230}$ and more disordered states, where the subdomains S1-H1-S2 and H2-H3 would adopt different packing from that of the native state, thus establishing distinct basins for those configurations.

In particular, CV 1 reflects the mobility and heterogeneity of the α-helix H1 in folded and misfolded conformations of PrP (11, 12). CVs 2 and 3 sample global properties of the protein structure to specifically discern between expanded and compact conformational states. Finally, CVs 4 and 5 are sensitive to the large scale motions between the two subdomains as well as the exposure of aggregation-prone regions.

Following the metadynamics protocol, Gaussian potentials were deposited every 5 ps, with a height of 0.4 kJ/mol. The width of the potential, σ, was set individually for each collective variable: σ_1 = 0.2 nm; σ_2 = 0.01 nm; σ_3 = 1.0; σ_4 = 0.03 nm; σ_5 = 1.0. We employed the well-tempered algorithm of metadynamics, which adapts the bias height

over time by a scaling parameter ΔT in order to reach a smoother convergence (13). The ΔT parameter is controlled by the bias factor γ, which was set to 10.

In order to generate the starting configurations, we energy minimized the NMR structure of huPrP$^{C}_{125\text{-}230}$ at pH 7.0 (PDB code 1HJM) (14). The T183A mutation was introduced using the MODELLER package (15). The proteins were solvated it in cubic boxes with a volume of 512.0 nm^3, with 16,039 Tip3p water molecules (16) and 3 sodium ions to neutralize the charge. Temperature was coupled at 310 K using the V-rescale algorithm (17), and equilibrated for 100 ps at constant volume with positional restraints of 1000 kJ/(nm^2 · mol) on the protein heavy atoms. Pressure was subsequently equilibrated at 1 atm using the Berendsen method (18), for another 100 ps with positional restraints. An initial sampling of 20 ns was carried out, and five configurations extracted every 2 ns from the second half of that sampling. Those five configurations were used as starting structures for the five bias-exchange metadynamics replicas. The metadynamics sampling was extended for 800 ns per replica, for both WT and T183A huPrP$^{C}_{125\text{-}230}$, resulting in a total sampling time of 8 μs.

The samplings were carried out in explicit water using the PLUMED 2.2 plugin (19) and the GROMACS 4.6.7 molecular dynamics engine (20). Protein molecules were modeled with the AMBER99SB-ILDN force field (21) and water molecules using the Tip3p model (16). The system was solvated in 16,039 waters and 3 sodium ions, resulting in a total number of atoms of 49,814 for WT huPrP$^{C}_{125\text{-}230}$ and 49,810 for the T183A variant. Electrostatic interactions were accounted with the Particle mesh Ewald method (22). The ensembles were run at constant pressure at 1 atm using the Berendsen algorithm (18) and constant temperature of 310 K using the V-rescale method (17). The LINCS algorithm (23) was used in defining the constraints and the integration timestep was set to 2 fs.

The convergence of bias-exchange metadynamics simulations is generally assessed by monitoring the evolution of the individual one-dimensional profiles for each collective variable (24). We evaluated the convergence of the sampling by monitoring the free energy difference (ΔG) between the two metastable basins identified in our study (huPrP$^{C}_{125\text{-}230}$ and huPrP*$_{125\text{-}230}$) as a function of time. As the simulation evolves convergence is expected for ΔG (25). In the case of WT, where the huPrP*$_{125\text{-}230}$ is not accessed as in the case of T183A, we chose the closest metastable basin to huPrP*$_{125\text{-}230}$ to monitor the simulations convergence (Figure S10), which is reached within the first

300 ns of sampling in each replica. In the case T183A, convergence was reached within 500 ns of each replica.

SI Figures

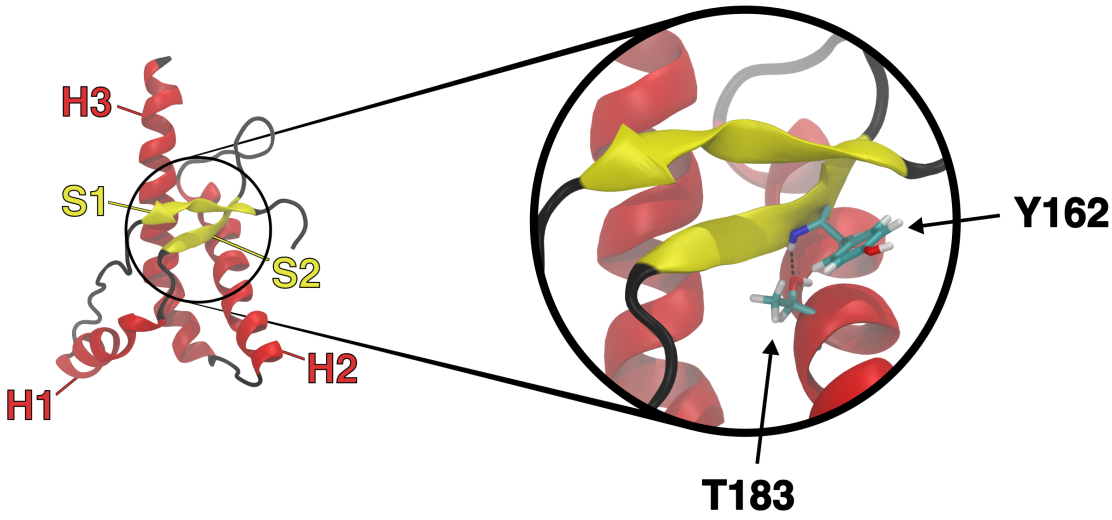

Figure S1. Native structure of huPrP$^{C}_{125\text{-}230}$. The structure, which was determined by NMR at pH 7 (PDB ID: 1HJM) (14), can be divided into two subdomains: S1-H1-S2 and H2-H3. A crucial hydrogen bond between the sidechain of T183 and the backbone amide of Y162 is highlighted in the close-up view.

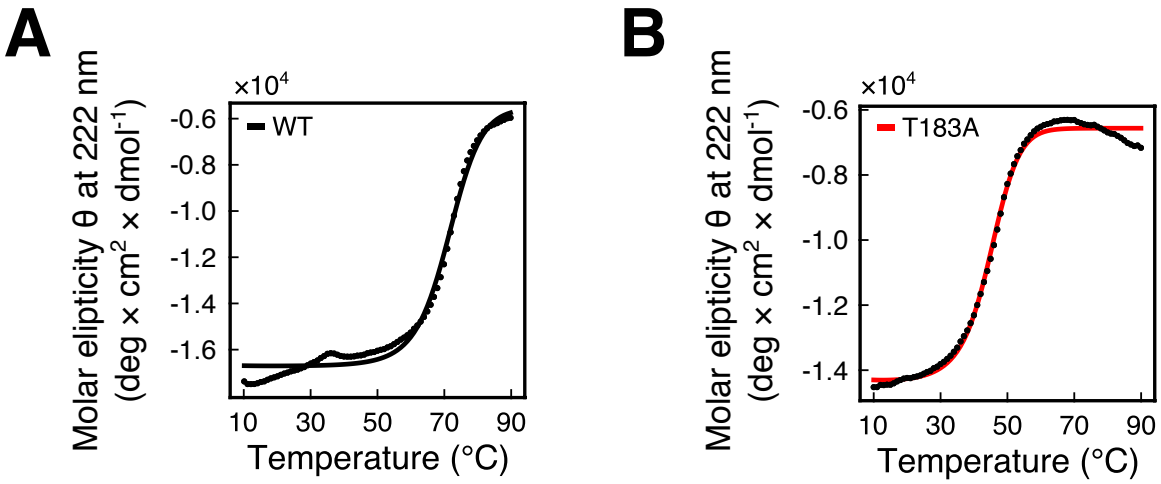

Figure S2. Unfolding curves of huPrP$^{C}_{125\text{-}230}$. Data were obtained by monitoring the CD values at 222 nm and analyzed according to a two-state Gibbs-Helmholtz model (26). **A**) WT huPrP$^{C}_{125\text{-}230}$. **B**) T183A huPrP$^{C}_{125\text{-}230}$.

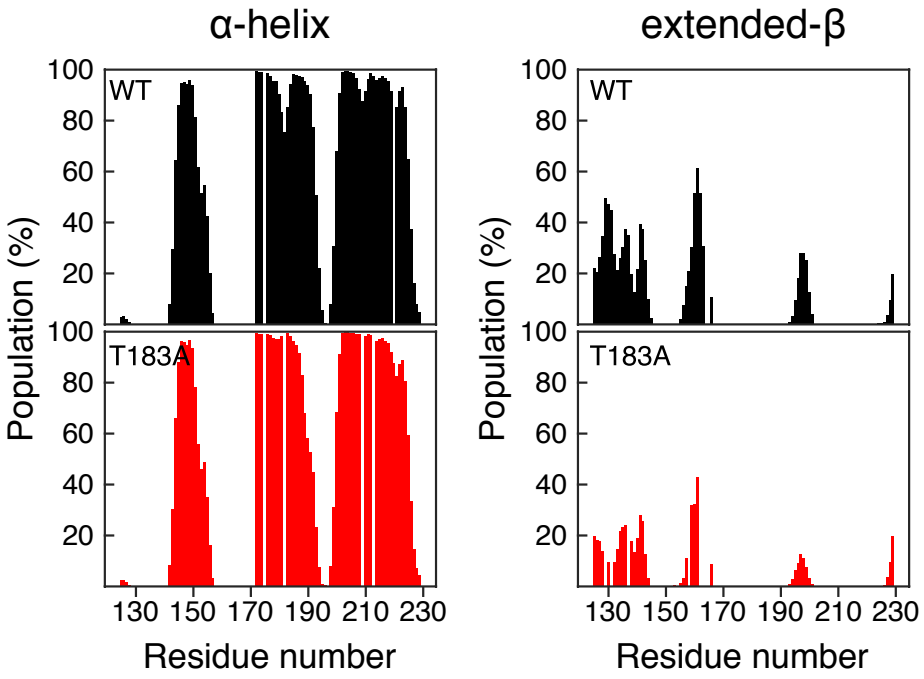

Figure S3. α-helix and extended-β populations in WT (black) and T183A (red) huPrP$^{C}_{125\text{-}230}$ from δ2D analysis of NMR chemical shifts.

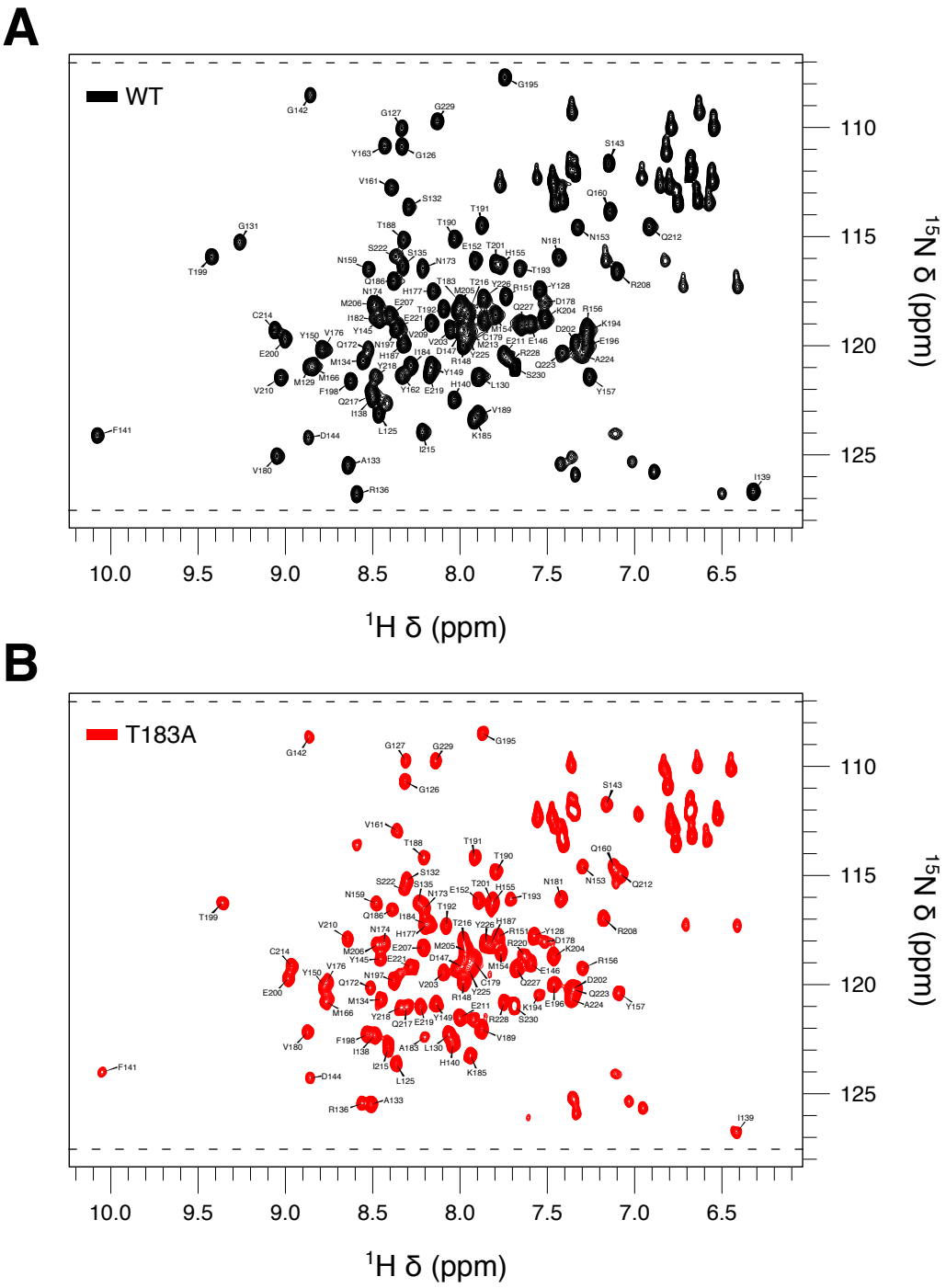

Figure S4. Assigned ^{1}H-^{15}N HSQC spectra of WT (A) and T183A (B) huPrP$^{C}_{125\text{-}230}$. Spectra were acquired and using an 800 MHz spectrometer at 16°C and pH 7.0. Protein samples were concentrated at 130 μM in 100 mM Na_2HPO_4 buffer.

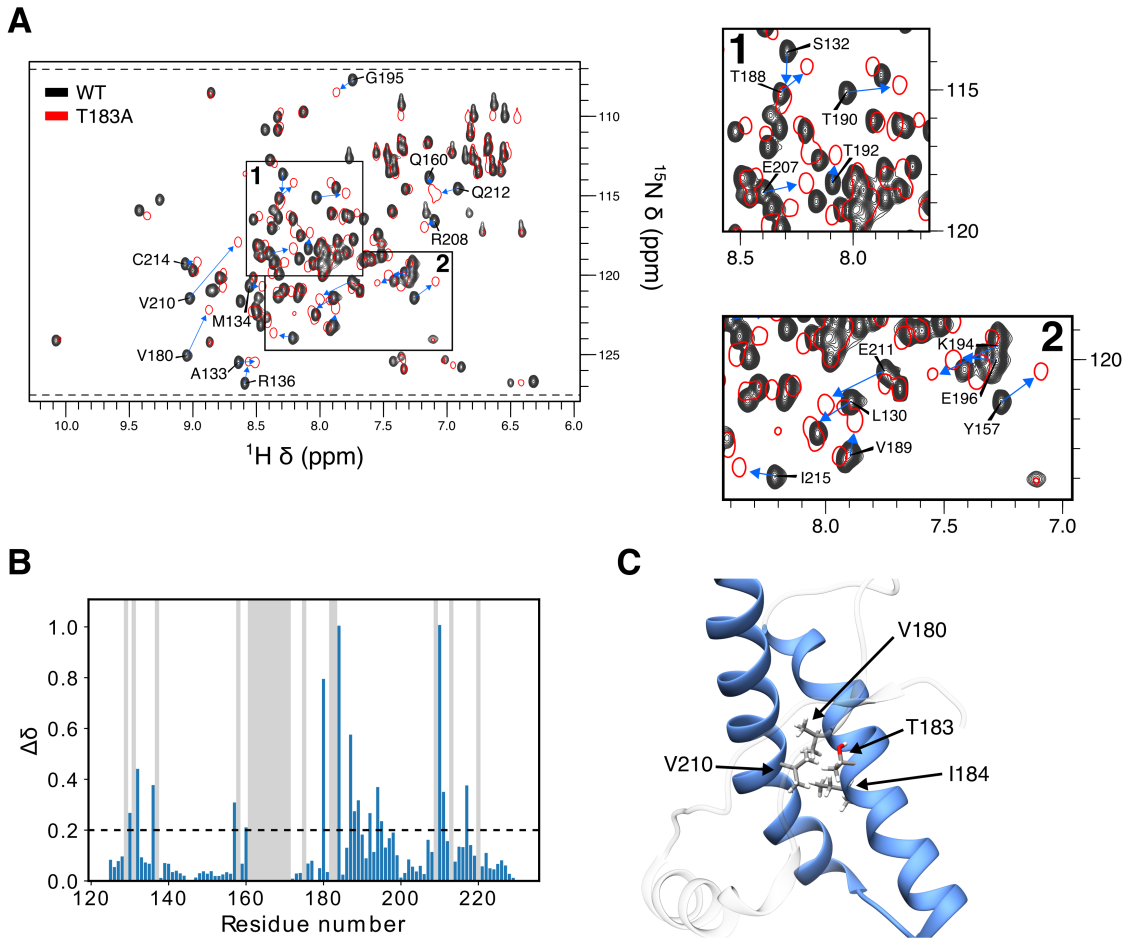

Figure S5. Chemical shift perturbations induced by the T183A mutation in huPrP$^{C}_{125\text{-}230}$. A) ^{1}H-^{15}N HSQC spectra of WT huPrP$^{C}_{125\text{-}230}$ (black) are shown with those of T183A huPrP$^{C}_{125\text{-}230}$ overlaid as single contour line (red). Major changes are labelled and noted with blue arrows. Spectra were acquired and using an 800 MHz spectrometer at 16°C and pH 7.0 in 100 mM Na_2HPO_4 buffer. **B**) Chemical shift perturbations ($\Delta\delta$) from the ^{1}H-^{15}N HSQC spectra plotted along the huPrP$^{C}_{125\text{-}230}$ sequence. Perturbations below the dashed line, at a value of 0.2, are considered to be minor. Missing residues are shaded in gray. **C**) V180, I184 and V210 are associated with the highest chemical shift perturbations. These residues form a hydrophobic patch directly adjacent to the mutated sidechain of T183.

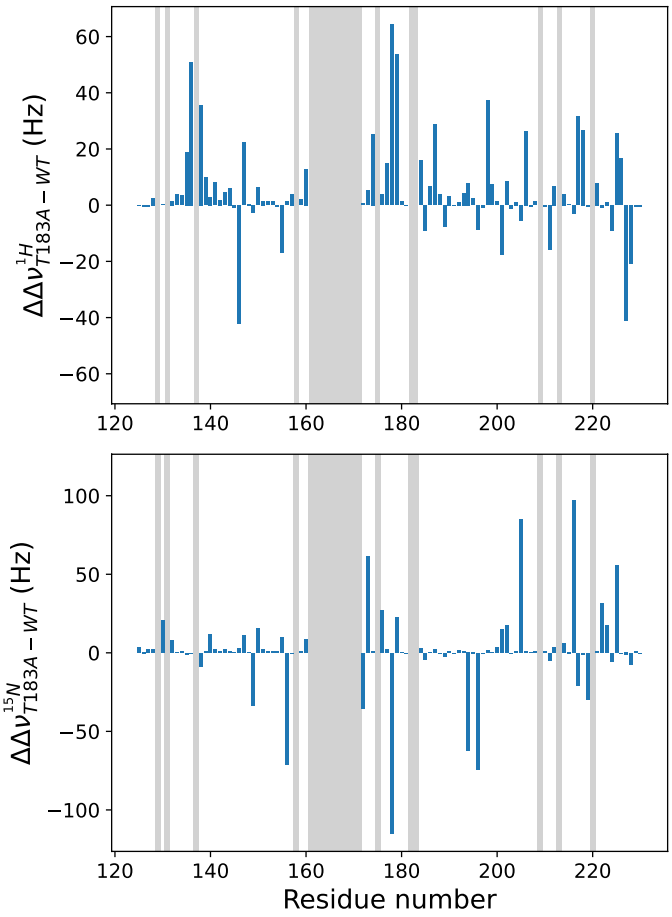

Figure S6. Perturbation of line widths in ^{1}H-^{15}N HSQC as a result of the T183A in huPrP$^{C}_{125\text{-}230}$. ΔΔν calculated as line widths of T183A minus those of the WT spectra are shown as a function of the residue number. Top and bottom panels report data for ^{1}H and ^{15}N atoms, respectively.

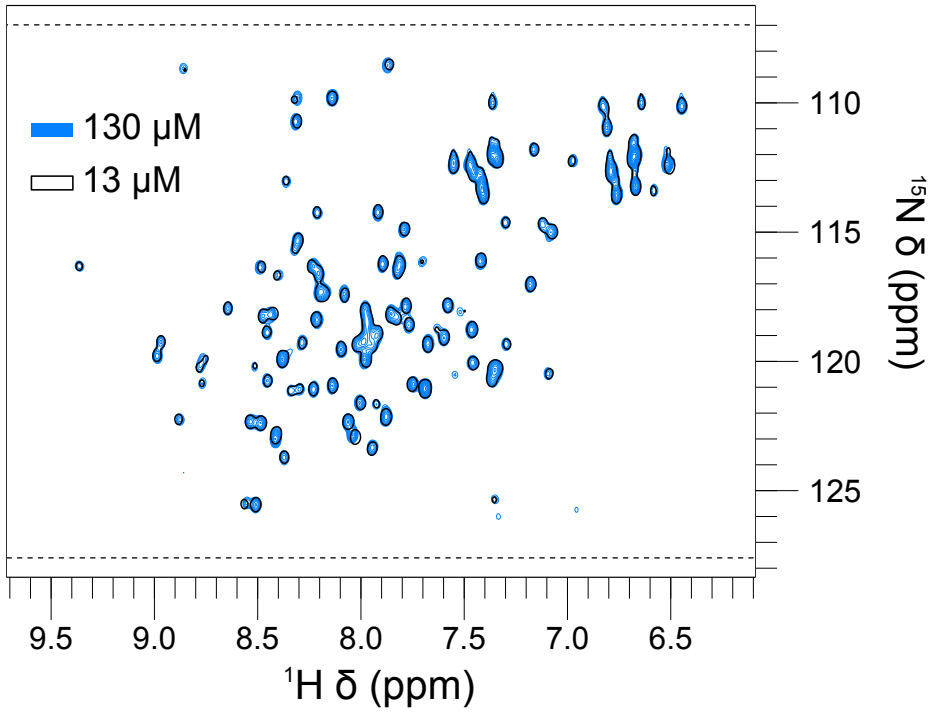

Figure S7. Dilution effects in the ^{1}H-^{15}N HSQC spectra of T183A huPrP$^{C}_{125\text{-}230}$. Spectra acquired using protein concentrations of 130 µM (blue) and 13 µM (black) are shown. The two spectra largely overlap, therefore for clarity the HSQC measured at a protein concentration of 13 µM is shown as a single contour line. Measurements were made at 16°C, pH 7.0 in 100 mM Na_2HPO_4 buffer using an 800 MHz spectrometer. The two spectra show highly similar line widths. In the ^{1}H, these are 42 ± 15 Hz and 41 ± 15 Hz, for 130 µM and 13 µM samples, respectively, whereas in the ^{15}N these are 51 ± 29 Hz and 51 ± 29 Hz.

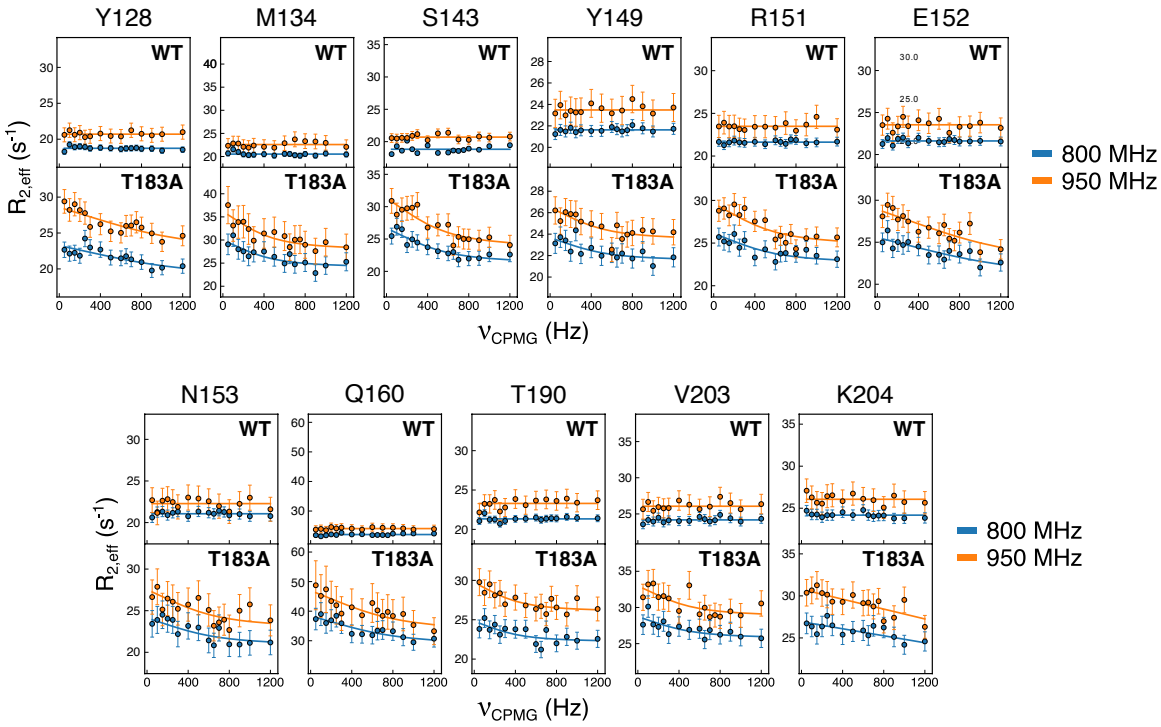

Figure S8. CPMG relaxation dispersion curves of huPrP$^{C}_{125\text{-}230}$. were measured at 800 MHz (blue) and 950 MHz (orange). Each panel corresponds to one residue found to be in conformational exchange in the T183A variant. No residue was found to be in exchange in the wild-type.

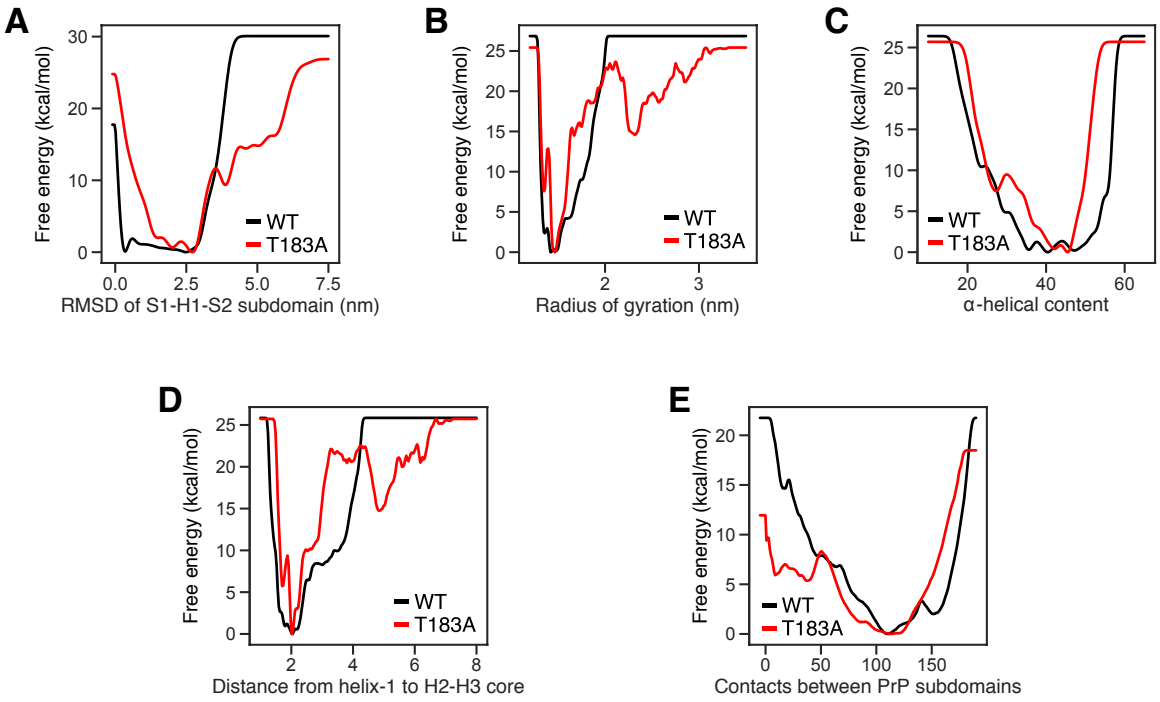

Figure S9. One-dimensional free energy landscapes from metadynamics samplings of huPrP$^{C}_{125\text{-}230}$. Wild-type and T183A huPrP$^{C}_{125\text{-}230}$ are shown in black and red, respectively. Free energy landscapes for each of the five collective variables employed in the bias-exchange setup are shown in panels A-E. (**A**) RMSD of the S1-H1-S2 subdomain calculated by superimposing huPrP$^{C}_{125\text{-}230}$ using the H2-H3 subdomain. **B**) Radius of gyration. **C**) Total α-helical content of the protein. **D**) Distance from H1 to the core of H2-H3. **E**) Cα contacts between the S1-H1-H2 and the H2-H3 subdomains.

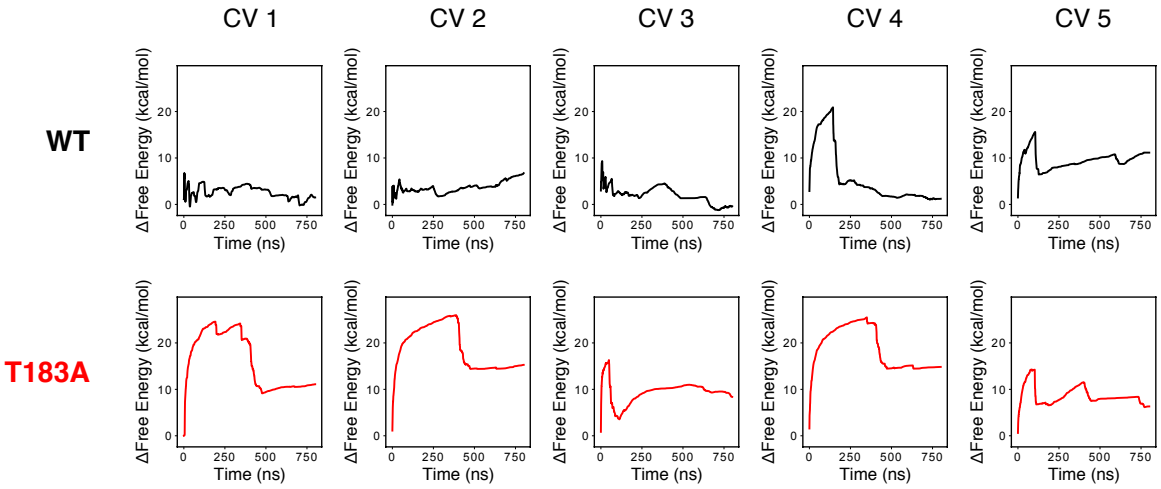

Figure S10. Convergence in bias-exchange metadynamics simulations. Convergence of the sampling was evaluated by following the free energy difference between the conformational states ($huPrP^{C}_{125-230}$ and $huPrP^{*}_{125-230}$) as a function of time. A reduction in the fluctuations of the free energy difference as time evolves suggests that the sampling has converged.

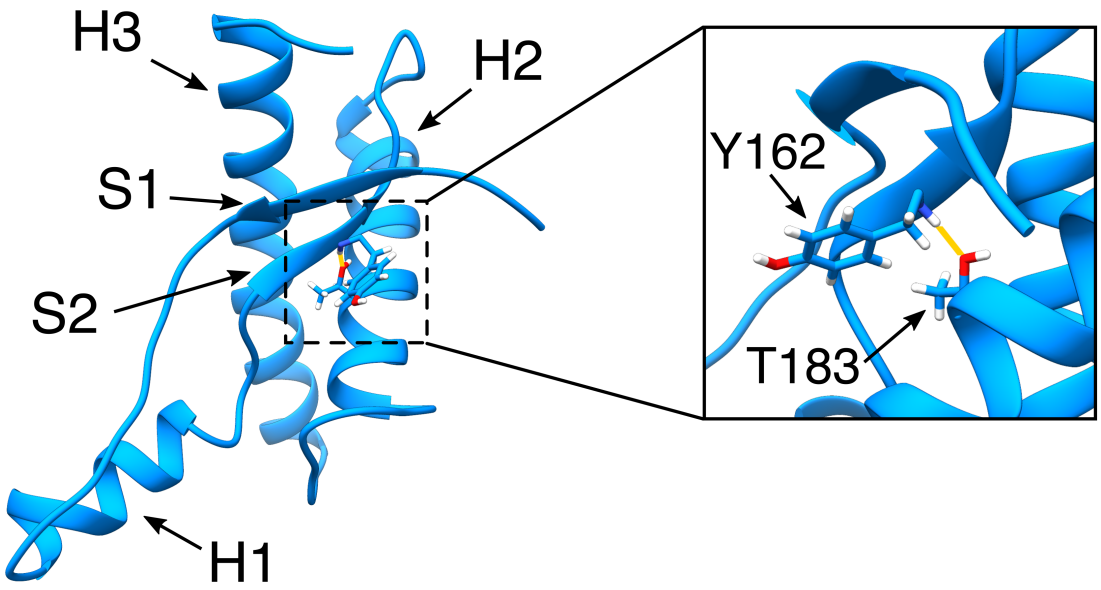

Figure S11. Large scale motions in the native WT huPrP$^{C}_{125\text{-}230}$. Rare conformational fluctuations of WT huPrP$^{C}_{125\text{-}230}$ induce partial detachment of the helix H1 from the native interface. Further detachment of the helix H1 from the H2-H3 subdomain are prevented by key interactions, including the H-bond between the side chain of T183 and main chain of Y162.

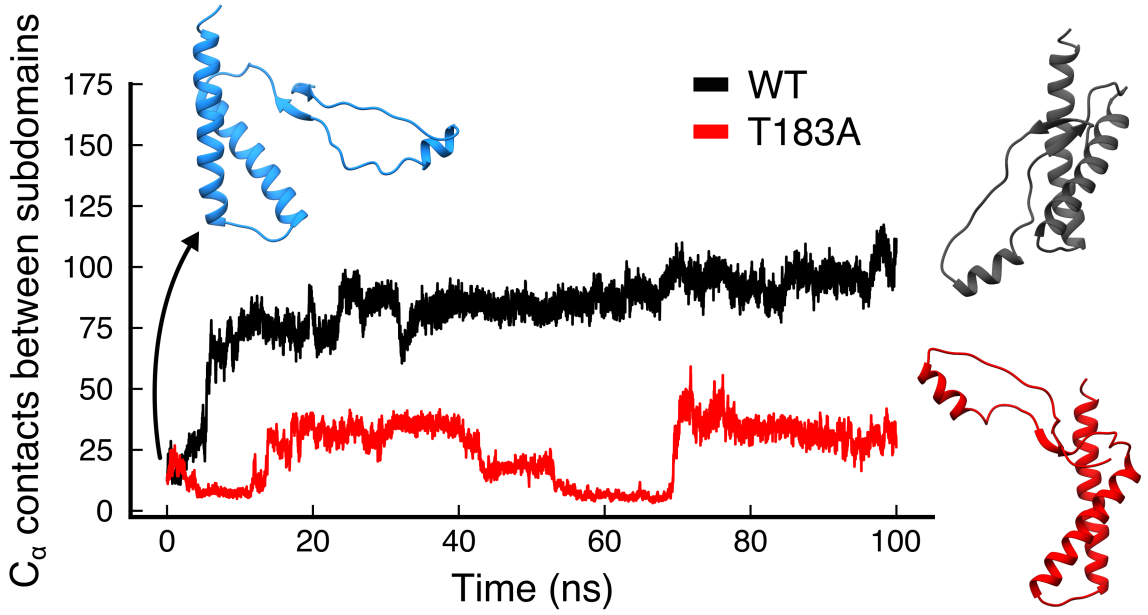

Figure S12. Unbiased MD simulations starting of WT and T183A huPrP*$_{125-230}$. Two simulations tarting from a representative structure of huPrP$^{*}_{125-230}$ were run for WT (black) and T183A (red) variants of huPrP. The WT starting conformation was obtained by reintroducing T183 in the structure of the mutant huPrP*$_{125-230}$. The simulations showed that WT huPrP*$_{125-230}$ is able to readily reform the native packing, which is estimated in this plot as the number of Cα contacts between the subdomains S1-H1-S2 and H2-H3 (i.e. as used in the CV5 of the metadynamics sampling). By contrast T183A was found to be unable to reform the native packing between the subdomains S1-H1-S2 and H2-H3 during the simulated time.

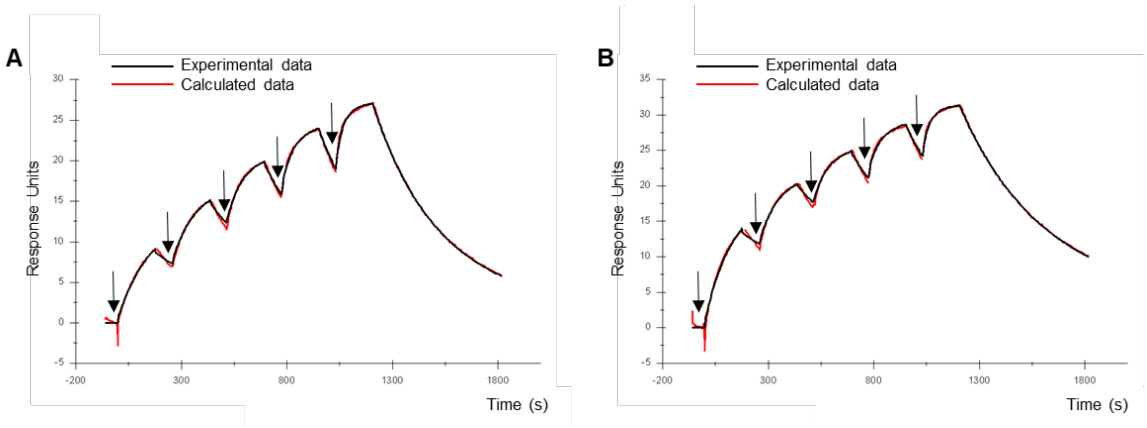

Figure S13. SPR sensorgrams. Binding affinity constants between POM1 scFv and WT (**A**) and T183A (**B**) huPrP$^{C}_{125\text{-}230}$ were determined by performing sequential injections of serial dilutions of WT and T183A (1.9 nM, 3.8 nM, 7.6 nM, 15 nM and 30.5 nM). Arrows indicate sample injections.

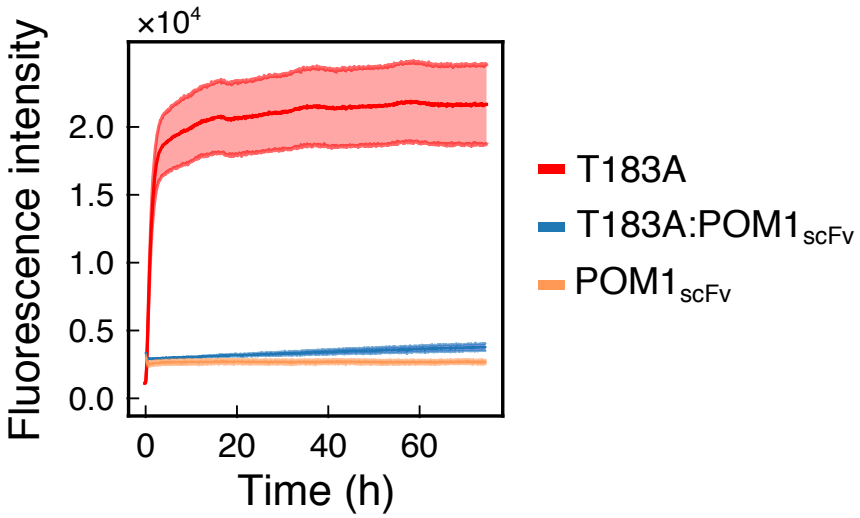

Figure S14. Single-chain variable fragment of POM1 suppresses T183A huPrP$^{C}_{125\text{-}230}$ aggregation. Thioflavin T (ThT) fluorescence was used to monitor the aggregation of T183A huPrP$^{C}_{125\text{-}230}$ alone (red) and in the presence of the POM1$_{scFv}$ (blue), which contains the antigen-binding variable regions of the antibody. The results show that POM1$_{scFv}$ is a potent suppressor of the aggregation of T183A huPrP$^{C}_{125\text{-}230}$. A ThT fluorescence control with POM1$_{scFv}$ alone is shown in orange.

Table S1. Thermodynamic parameters of huPrP$^{C}_{125\text{-}230}$ folding derived from circular dichroism melting curves analyzed with the Gibbs-Helmholtz model (26). ΔH_F and ΔG_F correspond to the folding enthalpy and free energy respectively.

	WT	**T183A**
Melting temperature (°C)	71.3	44.7
ΔH_F (kcal/mol)	-46.3	-44.2
ΔG_F at 37°C (kcal/mol)	-3.04	-0.94

Table S2. ^{15}N Chemical shift differences ($\Delta\omega$) between the major and minor states in CPMG experiments for residues in conformational exchange of T183A huPrP$^{C}_{125\text{-}230}$. Values were fitted with a 2-state model (4).

Residue	$\Delta\omega$ (ppm)
Y128	0.65
M134	2.30
S143	2.19
Y149	1.31
R151	1.70
E152	1.70
N153	1.63
Q160	3.03
T190	1.45
V203	1.57
K204	2.66

Table S3. Binding kinetics of POM1 scFv to WT and T183A huPrP$^{C}_{125\text{-}230}$ from analysis of SPR curves fitted with a 1:1 Langmuir and a heterogeneous ligand (hetLig) model.

Analyte	Model	k_{on}/ $M^{-1}s^{-1}$ (SD)	k_{off}/ $10^{-3}s^{-1}$ (SD)	KD/ nM (SD)	RU (max)
WT	1 + 1 Langmuir	(1.262 ± 0.002) x 10^6	2.575 ± 0.003	2.04	27.1
	hetLig	(6.20 ± 0.05) x 10^5	4.08 ± 0.02	6.56	18.2
		(2.57 ± 0.02) x 10^6	1.62 ± 0.01	0.61	11.9
T183A	1 + 1 Langmuir	(1.361 ± 0.002) x 10^6	2.478 ± 0.002	1.82	33.2
	hetLig	(8.60 ± 0.05) x 10^5	3.99 ± 0.01	4.64	26.0
		(3.08 ± 0.02) x 10^6	1.00 ± 0.001	0.33	10.7

SI References

1. G. Fusco, *et al.*, 1H, 13C and 15N resonance assignments of human muscle acylphosphatase. *Biomol. NMR Assign.* **6**, 27–29 (2012).
2. F. A. A. Mulder, N. R. Skrynnikov, B. Hon, F. W. Dahlquist, L. E. Kay, Measurement of Slow (μs−ms) Time Scale Dynamics in Protein Side Chains by 15 N Relaxation Dispersion NMR Spectroscopy: Application to Asn and Gln Residues in a Cavity Mutant of T4 Lysozyme. *J. Am. Chem. Soc.* **123**, 967–975 (2001).
3. F. Delaglio, *et al.*, NMRPipe: A multidimensional spectral processing system based on UNIX pipes. *J. Biomol. NMR* **6** (1995).
4. M. Tollinger, N. R. Skrynnikov, F. A. Mulder, J. D. Forman-Kay, L. E. Kay, Slow dynamics in folded and unfolded states of an SH3 domain. *J. Am. Chem. Soc.* **123**, 11341–52 (2001).
5. E. J. d'Auvergne, P. R. Gooley, Optimisation of NMR dynamic models I. Minimisation algorithms and their performance within the model-free and Brownian rotational diffusion spaces. *J. Biomol. NMR* **40**, 107–119 (2008).
6. C. Camilloni, A. De Simone, W. F. Vranken, M. Vendruscolo, Determination of secondary structure populations in disordered states of proteins using nuclear magnetic resonance chemical shifts. *Biochemistry* **51**, 2224–31 (2012).
7. M. P. Williamson, "Chemical Shift Perturbation" in *Modern Magnetic Resonance*, (Springer International Publishing, 2017), pp. 1–19.
8. A. Laio, M. Parrinello, Escaping free-energy minima. *Proc. Natl. Acad. Sci. U. S. A.* **99**, 12562–12566 (2002).
9. S. Piana, A. Laio, A bias-exchange approach to protein folding. *J. Phys. Chem.* **111**, 4553–4559 (2007).
10. F. Pietrucci, A. Laio, A collective variable for the efficient exploration of protein beta-sheet structures: Application to SH3 and GB1. *J. Chem. Theory Comput.* **5**, 2197–2201 (2009).
11. A. De Simone, A. Zagari, P. Derreumaux, Structural and hydration properties of the partially unfolded states of the prion protein. *Biophys. J.* **93**, 1284–92 (2007).
12. C. Camilloni, D. Schaal, K. Schweimer, S. Schwarzinger, A. De Simone, Energy landscape of the prion protein helix 1 probed by metadynamics and NMR. *Biophys. J.* **102**, 158–67 (2012).
13. A. Barducci, G. Bussi, M. Parrinello, Well-Tempered Metadynamics: A Smoothly Converging and Tunable Free-Energy Method. *Phys. Rev. Lett.* **100**, 020603 (2008).
14. L. Calzolai, R. Zahn, Influence of pH on NMR structure and stability of the human prion protein globular domain. *J. Biol. Chem.* **278**, 35592–35596 (2003).
15. N. Eswar, *et al.*, Comparative protein structure modeling using Modeller. *Curr. Protoc. Bioinforma.* **Chapter 5**, Unit-5.6 (2006).
16. W. L. Jorgensen, J. Chandrasekhar, J. D. Madura, R. W. Impey, M. L. Klein, Comparison of simple potential functions for simulating liquid water. *J. Chem. Phys.* **79**, 926 (1983).

17. G. Bussi, D. Donadio, M. Parrinello, Canonical sampling through velocity rescaling. *J. Chem. Phys.* **126**, 014101–7 (2007).

18. H. J. C. Berendsen, J. P. M. Postma, W. F. van Gunsteren, a DiNola, J. R. Haak, Molecular dynamics with coupling to an external bath. *J. Chem. Phys.* **81**, 3684–3690 (1984).

19. G. A. Tribello, M. Bonomi, D. Branduardi, C. Camilloni, G. Bussi, PLUMED 2: New feathers for an old bird. *Comput. Phys. Commun.* **185**, 604–613 (2014).

20. B. Hess, C. Kutzner, D. van der Spoel, E. Lindahl, GROMACS 4 : Algorithms for Highly Efficient , Load-Balanced , and Scalable Molecular Simulation. *J. Chem. Theory Comput.* **4**, 435–447 (2008).

21. K. Lindorff-Larsen, *et al.*, Improved side-chain torsion potentials for the Amber ff99SB protein force field. *Proteins* **78**, 1950–1958 (2010).

22. T. Darden, D. York, L. Pedersen, Particle mesh Ewald: An N log(N) method for Ewald sums in large systems. *J. Chem. Phys.* **98**, 10089 (1993).

23. B. Hess, H. Bekker, H. J. C. Berendsen, J. G. E. M. Fraaije, LINCS: A linear constraint solver for molecular simulations. *J. Comput. Chem.* **18**, 1463–1472 (1997).

24. F. Marinelli, F. Pietrucci, A. Laio, S. Piana, A Kinetic Model of Trp-Cage Folding from Multiple Biased Molecular Dynamics Simulations. *PLoS Comput. Biol.* **5**, e1000452 (2009).

25. A. Barducci, M. Bonomi, M. Parrinello, Metadynamics. *WIREs Comput. Mol. Sci.* **1**, 826–843 (2011).

26. N. J. Greenfield, Using circular dichroism collected as a function of temperature to determine the thermodynamics of protein unfolding and binding interactions. *Nat. Protoc.* **1**, 2527–2535 (2006).